Cell Prolif. 1998, **31**, 17–33

The morphological and spectral phenotype of apoptosis in HeLa cells varies following exposure to UV-C and the addition of inhibitors of ICE and CPP32

M. L. Miller, A. Andringa, J. Elliott, K. Conwell II, K. Dixon and M. P. Carty

Department of Environmental Health, University of Cincinnati, Cincinnati, USA

(*Received* 17 *December* 1997; *revision accepted* 23 *January* 1998)

Abstract. Numerous extra- and intracellular factors, including UV radiation, can initiate a programme of cell death by apoptosis. While apoptosis is commonly defined morphologically, the relationships between morphology and molecular events are not well established. To investigate these relationships in HeLa cells, eight morphometric criteria for cell proliferation and damage and 10 criteria for apoptotic phenotype were examined using light microscopy, and corroborated by ultrastructure and spectral imaging. They were identified (1) during a time course after irradiation with 0, 10 or 30 J/m^2 UV-C; (2) after separation of apoptotic from normal cells on a Percoll gradient; and (3) after irradiation with UV-C plus perturbation of the apoptotic pathway by treatment with inhibitors of two caspases, ICE and CPP32.

The number of cells in apoptosis increased in a dose-dependent manner after UV-C treatment. Centrifugation of irradiated cells on a Percoll gradient increased the collection of apoptotic cells tenfold. The stereotypical apoptotic phenotype, in which cells have deep cytoplasmic blebbing and highly condensed DNA, comprised only a few percent of all apoptoses, and was rarely seen in groups receiving caspase inhibitors. The most common apoptotic phenotype was a rounded cell with large spherical nucleolus and associated DNA. After treatment with UV-C plus inhibitors the apoptotic index was decreased by about 30% compared to UV-C radiation alone. These apoptotic cells had dark spherical cytoplasm with small blebs, greatly increased numbers of cytoplasmic ribosomes, abundant nucleolar material with a large separate granular component, and chromatin condensed at the nuclear membrane. Using the technique of spectral imaging, it was found that the spectrum obtained from the granular component of the nucleolus, which was elevated in apoptotic cells treated with UV-C plus inhibitors, was similar to the dense accumulation of ribosomes in the apoptotic cytoplasm. The data indicate that spectral imaging may be a useful tool for identifying and characterizing variations in the

Correspondence to: Dr M. L. Miller, Department of Environmental Health, University of Cincinnati, Cincinnati, OH 4526-0056, USA.

apoptotic process, and that the caspase inhibitors used here do not completely abolish UV-C induced apoptosis, but rather alter its incidence and progression.

Apoptosis is the manifestation of a plan for self-induced cell death. It is highly conserved through evolution and is involved in aspects of embryonic development, recognition of self, hormone-responsive cell growth and cell killing in some disease states (Wyllie, Kerr & Currier 1980, Buttyan 1991, Tomei 1991, Bishop *et al.* 1993, Sachs & Lotem 1993, Taylor 1993, Darzynkiewicz *et al.* 1995, Steller 1995, Thompson 1995, Touchette 1995, White 1996, Rowan & Fisher 1997). Genetic disregulation of modulators of apoptosis can have dramatic consequences, as seen in mice lacking or overexpressing factors such as p53 or Bcl-2 (Clark *et al.* 1993, Nakayama *et al.* 1993, Kroemer *et al.* 1995, Steller 1995, Miller *et al.* 1996). The complex biochemical processes of apoptosis as well as the various apoptotic phenotypes are currently being identified (Clarke 1990, Rowan & Fisher 1997). Yet, it is not clearly understood how interruptions in the numerous positive and negative modulators of this pathway impact the attendant varied and distinct apoptotic phenotypes (Wyllie *et al.* 1980, Clarke 1990, Kroemer *et al.* 1995, Vaux & Strasser 1996, Trump *et al.* 1997). It is important to understand the underlying mechanisms of apoptotis because it is essential for normal development and continuance, and is inextricably linked with cell proliferation (Cope & Willie 1991, McDonnell 1993, Baserga 1995, King & Cidlowski 1995, Skehan 1995, Stein *et al.* 1995). Knowledge of cell death also provides an opportunity for intervention in some human disease states (Dixon *et al.* 1997, Rudin & Thompson 1997).

A number of external stimuli, such as UV light, ionizing radiation, some carcinogens and viruses, and many other factors, are able to trigger apoptosis (Wyllie *et al.* 1980, Afshari & Barrett 1993, Corcoran *et al.* 1994, Solary *et al.* 1994, Miller *et al.* 1996). In addition, the list of modulators of the apoptotic process is lengthy and incomplete (Forbes *et al.* 1992, Falcieri *et al.* 1993, Raff *et al.* 1993, Lazebnik *et al.* 1993, 1995, Omerod *et al.* 1994). It is possible to envision a complex scenario which would allow entry, inhibition and exit from this pathway at numerous points, expressed as a wide variety of morphologies (Wyllie *et al.* 1980, Ramachandra & Studzinski 1995).

A family of cysteine proteases (caspases) has been identified as key effectors of the mammalian cell death pathway (Lazebnik *et al.* 1994, Rowan & Fisher 1997). Two of these proteases are interleukin-converting enzyme (ICE, caspase-1; Alnemri *et al.* 1996) and CPP32 (YAMA protease, caspase-3, apopain; Thompson 1995). The activation of ICE and CPP32 are interlinked, ICE being capable of activating CPP32, as well as itself, by proteolytic cleavage. CPP32 is also able to undergo autocatalysis. These and other ICE-like proteases, of which there at least 10, constitute critical factors in the control of the apoptotic pathway. Specific inhibition of these proteases has provided insight into whether interference with molecular events causes a significant change in apoptosis (Lazebnik *et al.* 1994, 1995, Tewari *et al.* 1995).

To begin to develop objective criteria for identification and classification of the morphological features of apoptosis, we have applied several techniques. Light and electron microscopic morphological characteristics of apoptosis, occurring after UV-C irradiation of cultured HeLa cells and after the addition of inhibitors of ICE and CPP32, were quantified to correlate important molecular events in apoptosis with specific subcellular phenotypes. Additional information on the phenotype of the apoptotic cells, particularly the state of DNA and the distribution of RNA, was obtained by using spectral imaging, thus enhancing the information derived from the toluidine blue stained microscopic sections. Combining these

techniques revealed that the apoptotic structures identified by light and electron microscopy can also be characterized on the basis of their spectral characteristics.

MATERIALS AND METHODS

Cell culture and exposure

HeLa cells were grown at 37°C and 5% CO_2 in Dulbecco's modified essential medium (DMEM) supplemented with 10% fetal bovine serum. Medium was removed and conserved, cells were covered with phosphate buffered saline (PBS), pH 7.4 and exposed to UV-C radiation from a mercury vapour lamp with an emission maximum at 254 nm (UV Products, Upland, CA) for a dose of 0, 10 or 30 J/m^2. Following irradiation cells were washed once with PBS and the conserved medium was replaced. Cells were either fixed 0, 8, 18 or 24 h after irradiation, or further exposed to 100 μM Z-VAD-FK (Kamiya Biomedical Co., Thousand Oaks, CA) and/or 100 μM Z-DEVD-FK, inhibitors of ICE (caspase-1) and CPP32 (caspase-3), respectively. Cells were fixed after 18 h in culture. To amplify the collection of apoptotic cells from the treated cell population, some samples were separated on gradients as follows: cell pellets were resuspended in 400 μl of PBS and layered onto a gradient of 48% to 65% Percoll in a 15 ml glass tube. Gradients were centrifuged at $23000 \times g$ in a SS34 Sorvall rotor for 2 h at 4°C. The major sharp band of cells, in both untreated and UV-C treated cells, which sedimented with a buoyant density of 1.03–1.04 g/ml, was collected and labelled the top fraction. Cells with a buoyant density of 1.05–1.077 g/ml were collected as the bottom fraction. Buoyant density was determined from density marker beads run at the same time on parallel gradients. There was no bottom fraction in the untreated cell population.

Preparation of cells for morphological analysis

Zero, 8, 18 and 24 h after exposure to UV-C, with and without inhibitors, HeLa cells were washed once with PBS, collected with a plastic scraper, pelleted at $1000 \times g$ for 5 min, resuspended in a small volume of PBS in a conical Beem® capsule and centrifuged at $1000 \times g$ for 5 min. Fixative (4% paraformaldehyde in phosphate buffer, pH 7.4) was gently layered onto the pellets. Tissue pellets were fixed overnight, postfixed in 1% osmium tetroxide for 2 h, dehydrated through a graded ethanol series (30, 50, 70, 85, 95 and 100%), propylene oxide and embedded in Spurr's resin. One micron thick sections were stained with toluidine blue for light microscopy. Blocks were sectioned several times at 10–20 μm intervals, and morphometric and spectral values for each category of cell were obtained from the separate sections. These data were pooled to minimize any bias generated within the cell pellet during centrifugation. Thin sections, serial to the sections for light microscopy, were placed on copper grids, and stained with uranyl acetate and lead citrate for transmission electron microscopy (TEM).

Morphometry

Morphological categories were selected to reflect cell proliferation and cell death. Cells were counted using a Zeiss Photomicroscope at $1250 \times$. Specifically, normal HeLa cells contained intact nuclei with little to no condensed chromatin, blebbing, extensive vacuolization, or condensation of cytoplasmic or nuclear contents. Cells without nuclei were not counted. HeLa cells with a considerably darker cytoplasm than neighbouring cells, but containing a nucleus with typical patterns of chromatin condensation (and/or a typical nucleolus) were categorized as dark cells. Necrotic cells had cytoplasm and nuclei which were grossly vacuolated and darkly stained, and cellular membranes appeared to be ruptured. Multinu-

cleate cells contained two to several nuclei, appearing either separate or lobular. Mitotic cells were identified by condensed chromosomes in prometaphase to late anaphase in the absence of a nuclear membrane. Cells with deeply invaginated nuclei were considered to be amitotic (Weiss 1984). In some cells the condensation of nuclear material resembled that of a cell in late prophase, with a band of condensed chromatin spanning more than half of the nucleus, as if duplicated chromosomes were ready to separate. The nuclear membrane was still intact in these cells, and these were referred to as cells in G_2/M. Cells with ring-shaped (doughnut shaped) nucleoli were considered less active in terms of RNA synthesis, because of the presence of a single (or few) fibrillar centres (Schwarzacher & Wachtler 1993).

Apoptotic cells had pools of chromatin or severe cytoplasmic shrinkage with blebbing or both (Wyllie *et al.* 1980). There was wide variety in the morphological characteristics of apoptotis in the experimental groups. This category was, therefore, subdivided depending upon the presence or absence of specific morphology. A total of more than 1300 apoptotic cells were evaluated. The incidence of apoptotic cells overall was counted and the percentage of apoptotic cells, with the following characteristics was calculated (Tables 1–5): apoptotic cells (1) with cell membranes with small blebs; (2) with prominent and deep blebs at one pole only; (3) with deep cytoplasmic blebs over the entire surface; (4) with areas of peripheral, highly condensed, DNA within the nucleus (corresponding to digested DNA); (5) with a prominent granular component of the nucleolus; (6) with large spherical condensation of nucleolar structures and associated DNA; (7) with nuclei with small clumps of highly condensed chromatin, more or less evenly sized and spaced at the inner nuclear membrane; and (8) active nucleoli containing numerous large fibrillar centre(s) (representing active transcription and processing of pre-rRNA and mRNA).

Spectral imaging

Spectral imaging is a novel technique which can increase the amount of information gained from tissue sections stained with conventional methods. To further characterize morphological features observed by light and electron microscopy, spectral imaging of normal cells and cells in apoptosis was used to identify apoptotic DNA, RNA in the nucleus, and the ribosomes within the cytoplasm from the same sections utilized for light microscopy and

Table 1. Mean peak of the spectral signatures for selected cytoplasmic and nuclear structures in unaffected and apoptotic HeLa cells

Structure	Mean nm $\pm$ SEM	$P \leqslant 0.01$
Background (j) white	546.1 $\pm$ 0.48	a,b,c,d,e,f,g,h,i
Cytoplasm (i) light green	534.18 $\pm$ 1.2	a,b,c,f,g,h,j
Nucleoplasm (d) yellow	535.6 $\pm$ 1.3	a,b,c,e,f,g,h,j
Peripheral chromatin (f) turquoise	522.0 $\pm$ 2.0	a,b,c,d,h,i,j
Nucleolus (dense fibrillar (a) dark blue)	504.21 $\pm$ 2.5	c,d,e,f,g,h,i,j
Nucleolus (fibrillar centre (b) green)	515.5 $\pm$ 1.9	a,c,d,f,h,i,j
Cytoplasm light (h) grey*	530.1 $\pm$ 1.1	a,b,c,d,e,f,g,i,j
Cytoplasm-ribosomes (g) orange*	516.8 $\pm$ 2.17	a,c,d,h,i,j
Pale nucleoplasm*	527.4 $\pm$ 1.6	a,b,c,d,e,f,g,i,j
Nucleolar granular component (e) pink*	516.7 $\pm$ 1.77	a,c,d,e,f,h,i,j
DNA (c) red*	492.2 $\pm$ 1.6	a,b,c,d,e,f,g,h,i,j

n=26 cells examined spectrally. Each cell profile contained most subcellular component listed above.

*Apoptotic cells.

Table 2. Cytoplasmic phenotypes. Percentage of cytoplasmic characteristics in the total population of apoptotic cells seen in response to irradiation with 0, 10 and 30 J/m^2 UV-C, with and without caspase inhibitors. The phenotypes were sorted into three categories: (1) cells with rounded cytoplasm with none, to a few, small blebs; (2) cells with rounded cytoplasm with only the apical portion showing deep blebs; and (3) cells where the entire cytoplasm showed deep blebs

J/m^2	Hours	Rounded, small blebs	Deep apical blebs	Deep blebs overall
0	All	71.1	11.1	17.8
0	Inh*	67.6	16.2	16.2
10	0	75.0	25.0	0
10	8	37.5	62.5	0
10	24	75	16.7	8.3
30	0	72.7	9.1	18.2
30	8	47.6	23.8	28.6
30	18	82.1	5.8	12.1
30	18 Inh	81.8	14.3	3.9
30	24	71.7	21.7	6.5

*Inh=inhibitors of ICE, CPP32, or ICE and CPP32 together.

morphometry. The morphology of the organelles of interest was determined with electron microscopy and the spectra was determined from the same or similar cells, on serial sections, using an Applied Spectral Imaging spectrophotometer with SpectraCube software. This equipment provided a spectral plot from 450 to 700 nm of each pixel of an image captured by a cooled CCD camera and an interference spectrophotometer. A Fourier transform was calculated for each of these pixels and the information displayed as intensity at each nanometre. Areas of interest were analysed spectrally and highlighted with digital colour as follows: (a) normal dense fibrillar component of the nucleolus, deep blue; (b) fibrillar centre of the normal nucleolus, green; (c) apoptotic DNA, red; (d) nucleoplasm from unaffected cells, yellow; (e) dense apoptotic cytoplasm, pink; (f) normal peripheral condensed chromatin, turquoise; (g) apoptotic granular component of the nucleolus, orange; (h) light apoptotic cytoplasm, grey; (i) cytoplasm from unaffected cells, light green; (j) background, white. Apoptotic cells were analysed as pairs with adjacent unaffected HeLa cells. Files were captured using a fast scan, multi-format, Hamamatsu C4880-85 camera, a Nikon Eclipse

Table 3. Nuclear phenotypes. Percentage of apoptotic cells having nuclei with and without small peripheral clumps of highly condensed DNA

J/m^2	Hours	Without peripheral clumps of chromatin	With regularly shaped peripheral clumps of chromatin
0	All	91.1	8.8
0	Inh*	47.3	52.7
10	0	100	0
10	8	75	25
10	24	84.5	12.5
30	0	81.8	18.2
30	8	81	19
30	18	77.2	22.8
30	18 Inh	11.4	88.1
30	24	84.8	15.2

*Inh=inhibitors of ICE, CPP32, or ICE and CPP32 together.

Table 4. Nuclear phenotypes. Percentage of apoptotic cells with nuclei with and without nucleolar structures

J/m^2	Hours	Without nucleoli	Prominent granular component	Nucleoli with fibrillar centres
0	All	86.7	0	13.3
0	Inh*	93.2	2.7	4.1
10	0	100	0	0
10	8	50	0	50
10	24	58.3	0	41.7
30	0	54.5	0	45.5
30	8	71.4	0	28.6
30	18	92.9	1.1	6.0
30	18 Inh	91.2	6.8	2.1
30	24	65.2	0	34.8

*Inh=inhibitors of ICE, CPP32, or ICE and CPP32 together.

E800 light microscope, at $\times 1000$, and processed using SPCube® software (ASI, Applied Spectral Imaging, San Diego, CA). Images were captured as raw data. Red, green and blue (RGB) values were set at 600–700 nm, 500–600 nm and 450–500 nm, respectively. Five to 10 spectra were recorded from each of the 10 areas of interest for each cell image. Using the zoom window, a single pixel was selected which was representative of the average of these 5–10 spectra for use in classification of the spectral data. Noise level, intensity and gradient options were set at default values (1.0, 0.001 and 1.0, respectively), and images were classified without normalization. Classified images, matching RGB images, with pixels of interest marked, and spectral plots were saved as .tif files. These were paired with corresponding electron micrographs for analysis (Figure 1).

Table 5. Nucleolar phenotypes. Percentage of apoptotic cells with (1) exaggerated granular component of the nucleolus (peak spectrum about 516 nm); (2) large nucleolus and associated DNA (peak spectrum about 504 nm); and (3) peripheral, pooled highly fragmented DNA (peak spectrum about 492 nm)

J/m^2	Hours	Granular component	Nucleolus and associated DNA	Highly fragmented DNA
0	All	13.3	53.3	11.1%†
0	Inh*	39.2	36.5	0
10	0	0	100	0
10	8	12.5	75	0
10	24	4.2	41.7	33.3
30	0	9.1	54.5	0
30	8	14.3	52.4	4.8
30	18	13.2	54.4	18.1
30	18 Inh	66.8	9.6	1.3
30	24	17.4	47.8	8.7

*Inh=inhibitors of ICE, CPP32, or ICE and CPP32 together.

†A percentage of the apoptotic cells in each group had nucleolar phenotypes which fell into categories other than those above.

Data analysis

For the morphometric data derived from the light microscope and electron micrographs, means, standard deviations, errors of the mean and *P* values were generated with the General Linear Model using Statistical Analysis System (SAS) for the PC. A Student's *t*-test was used for determining significant differences in values for spectral peaks among cells (Sigma Plot, Jandel Scientific, Rancho Cordova, CA). Differences were considered significant when $P \leqslant 0.05$.

RESULTS

Quantitation of HeLa cell proliferation and damage after UV-C exposure

The percentage of cells in mitosis, G_2/M and apoptosis was affected by UV-C in a dose-dependent manner. Mitotic idex was lowest 8 h after 10 J/m^2 UV-C and subsequently increased, resulting in significantly more mitoses than in control cultures by 24 h after exposure (Figure 2). Thirty J/m^2 maximally depressed the mitotic index at 18 h, slightly later than the maximal depression in the 10 J/m^2 UV-C group (Figure 2).

Eight through 24 h after 30 J/m^2 UV-C the number of cells in G_2/M was significantly decreased compared to controls. This depression was more persistent and less variable than mitotic index. A diminished number of cells in G_2/M was usually accompanied by a depression in the mitotic index, and when G_2/M cells were increased the mitotic index tended to follow (Figure 2).

Other measures of cell proliferation and damage, such as multinucleate and dark cells, cells with irregular nuclear membranes and in amitosis (cleft nuclei) (Tables 6 and 7), and those with ring-shaped nucleoli with few fibrillar centres (less active RNA synthesis) were not significantly different among the UV-C groups and the unirradiated controls.

Apoptotic cells were identified by the morphological and spectral characteristics defined in the Materials and Methods section (Figure 1). The incidence of apoptotic cells was not significantly increased in HeLa cells after 10 J/m^2 UV-C at 0, 8, 18 or 24 h, but was significantly increased at 18 h after 30 J/m^2 UV-C (Figure 2).

The UV-C irradiated HeLa cells fractionated on a Percoll gradient provided cell populations which were highly enriched in apoptotic cells, greatly facilitating the morphometry. Comparing the untreated HeLa cells (whole cell pellet, $n=8$) and the top fraction of these cells (top band on Percoll gradient, $n=1$) there were no significant differences in mitotic index, or apoptoses. At 18 h after irradiation at 30 J/m^2 UV-C, the mean number of apoptotic cells, pooled from all experiments, was about 30%. Total damage was significantly increased

Figure 1. Three examples of different apoptotic phenotypes are given in this figure, and two unaffected HeLa cells in the same field are seen adjacent to apoptotic cells in the right and left sets. The phenotypes from left column to right are (a, d, g) early apoptosis, (b, e, g) apoptosis in the presence of inhibitors of the caspases, and (c, f, i) late phase apoptosis. The panel (a–c) shows RGB images which are generated from the raw spectral images. The small squares on those images mark the pixels from which the spectra were derived. These areas were then ascribed digital colours (a–j in Table 1). The images (d–f) were 'classified' according the spectra assigned to a through j, and all pixels with similar spectra were digitally coloured accordingly. Black represented those pixels for which a reasonable fit could not be found. Light colours were chosen for unaffected cytoplasmic and nuclear structures, while dark and intense colours were chosen for apoptotic structures. It is easily seen that there are spectral uniqueness in the apoptotic cells versus the unaffected cells. In this figure, the RGB image is immediately above its own classified image, and an electron micrograph of an equivalent cell is below (g–i). Magnification of the RGB and classified images was 1000× at the microscope. The magnification of electron micrographs is 2500×.

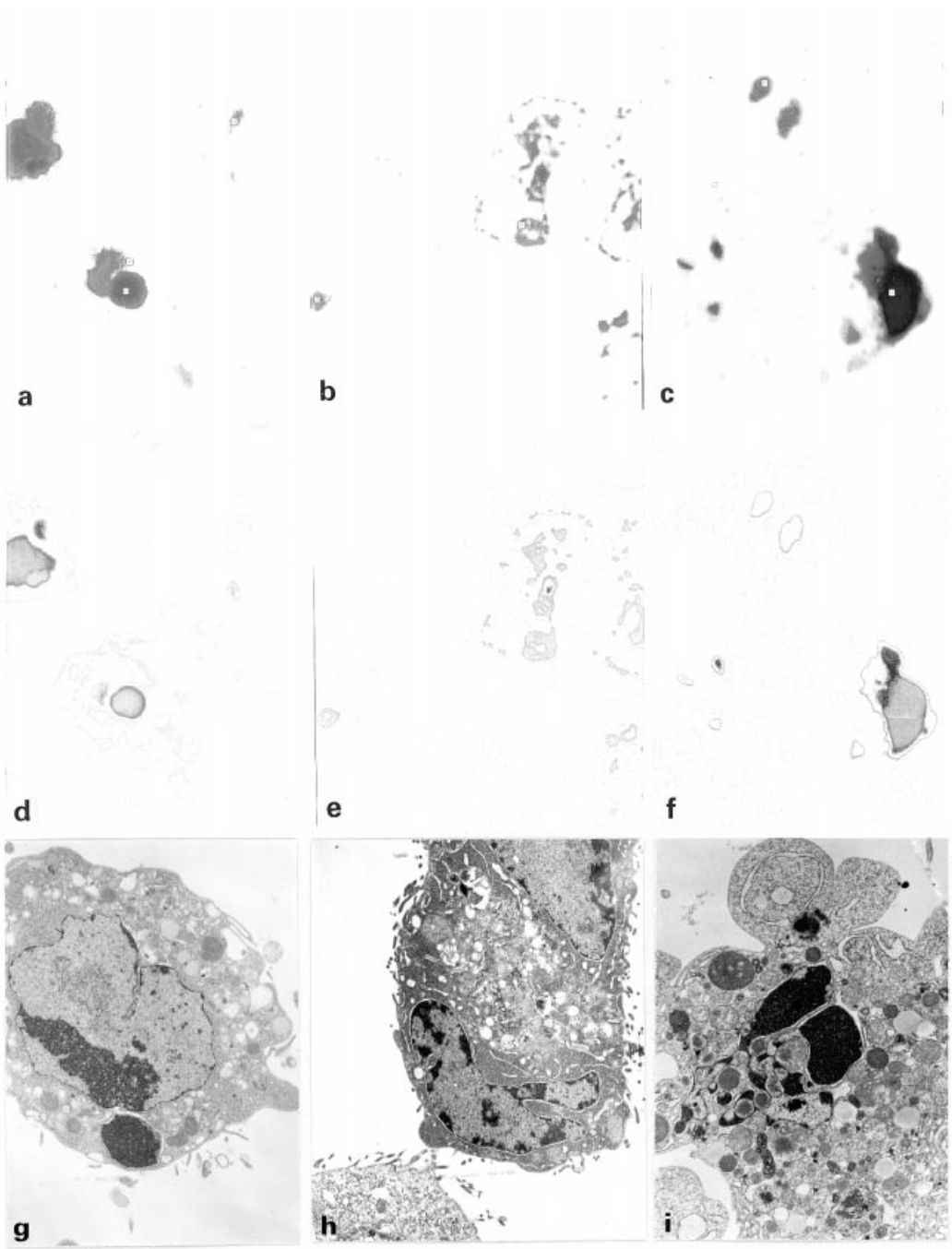
a
b
c
d
e
f
g
h
i

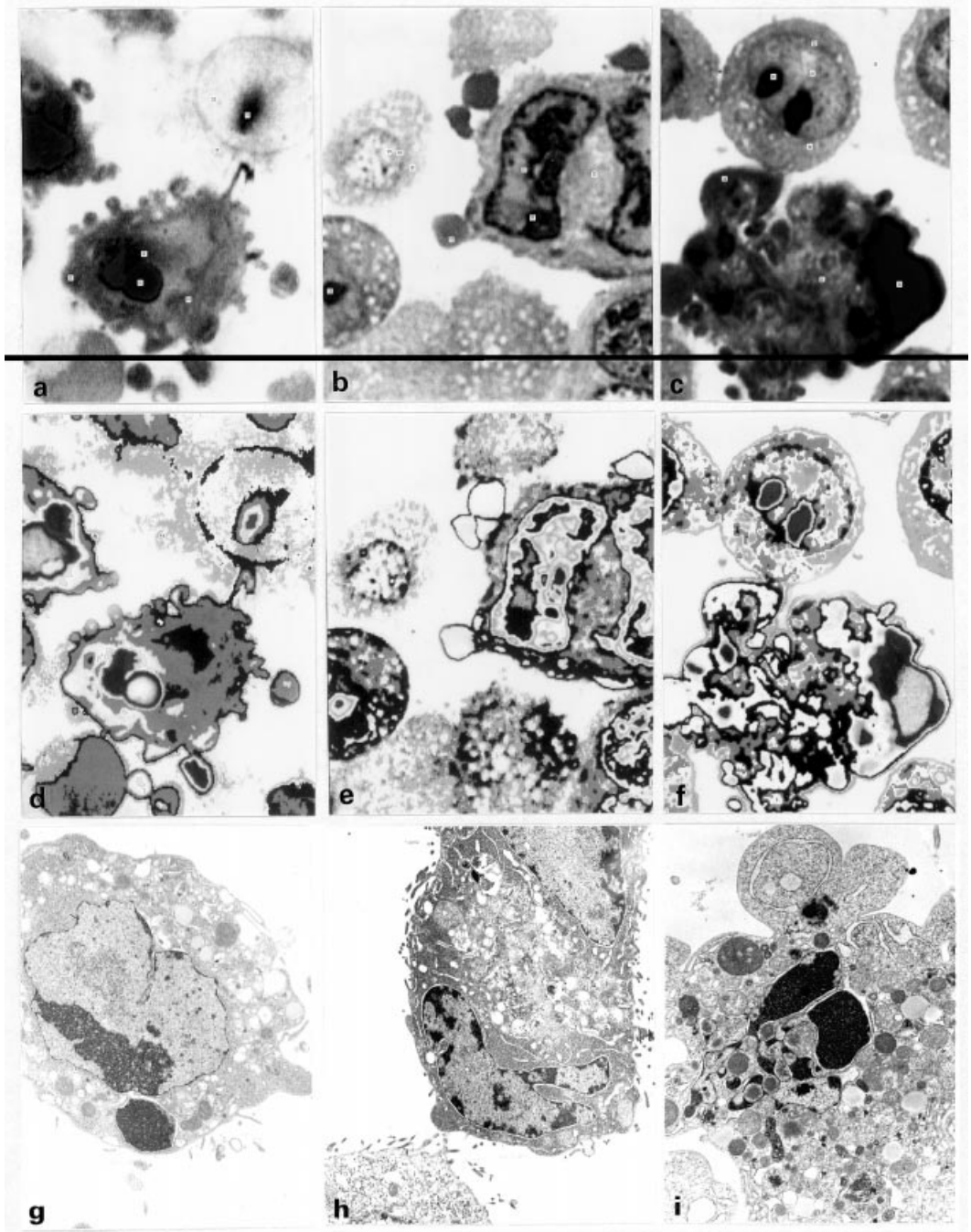
a
b
c
d
e
f
g
h
i

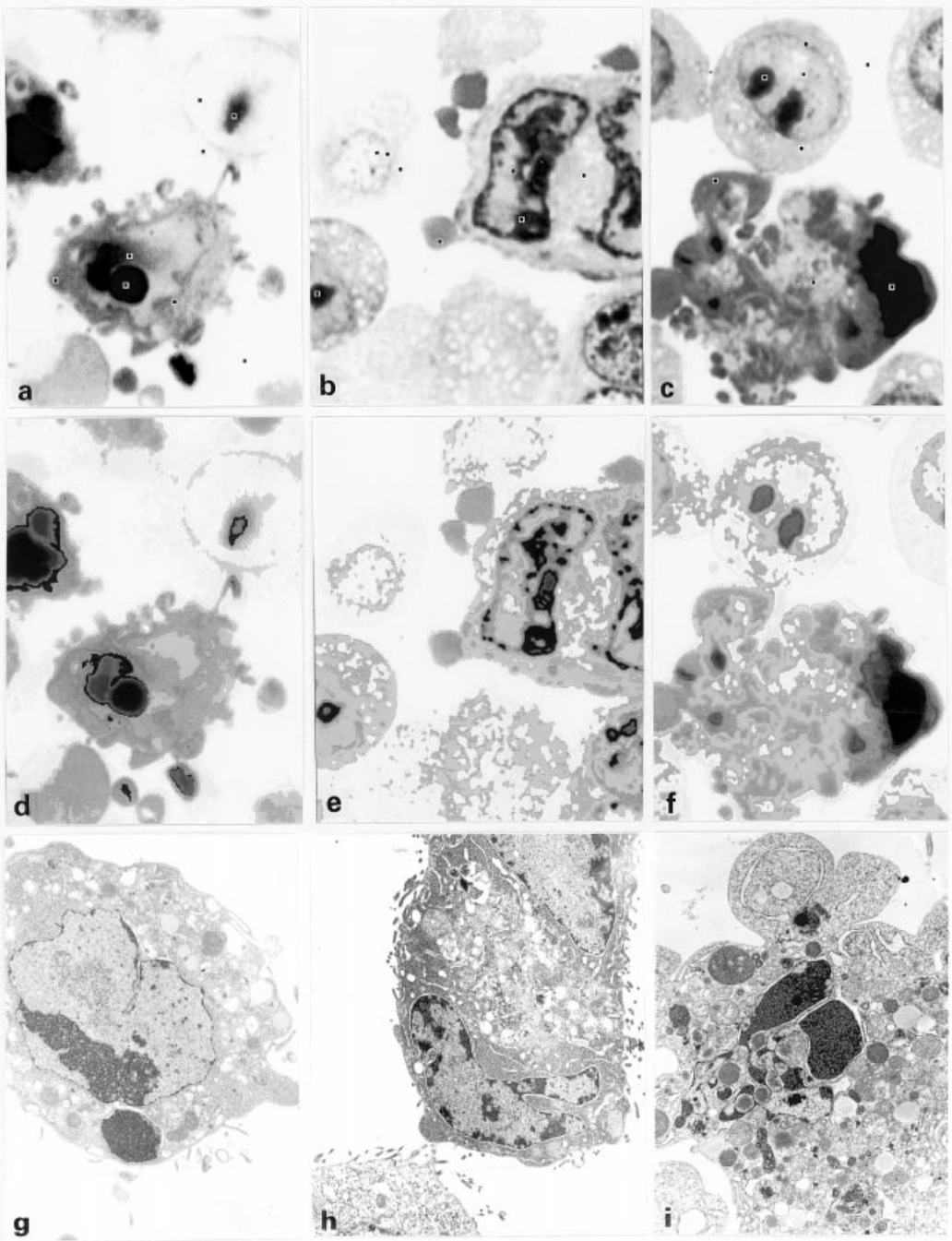
a
b
c
d
e
f
g
h
i

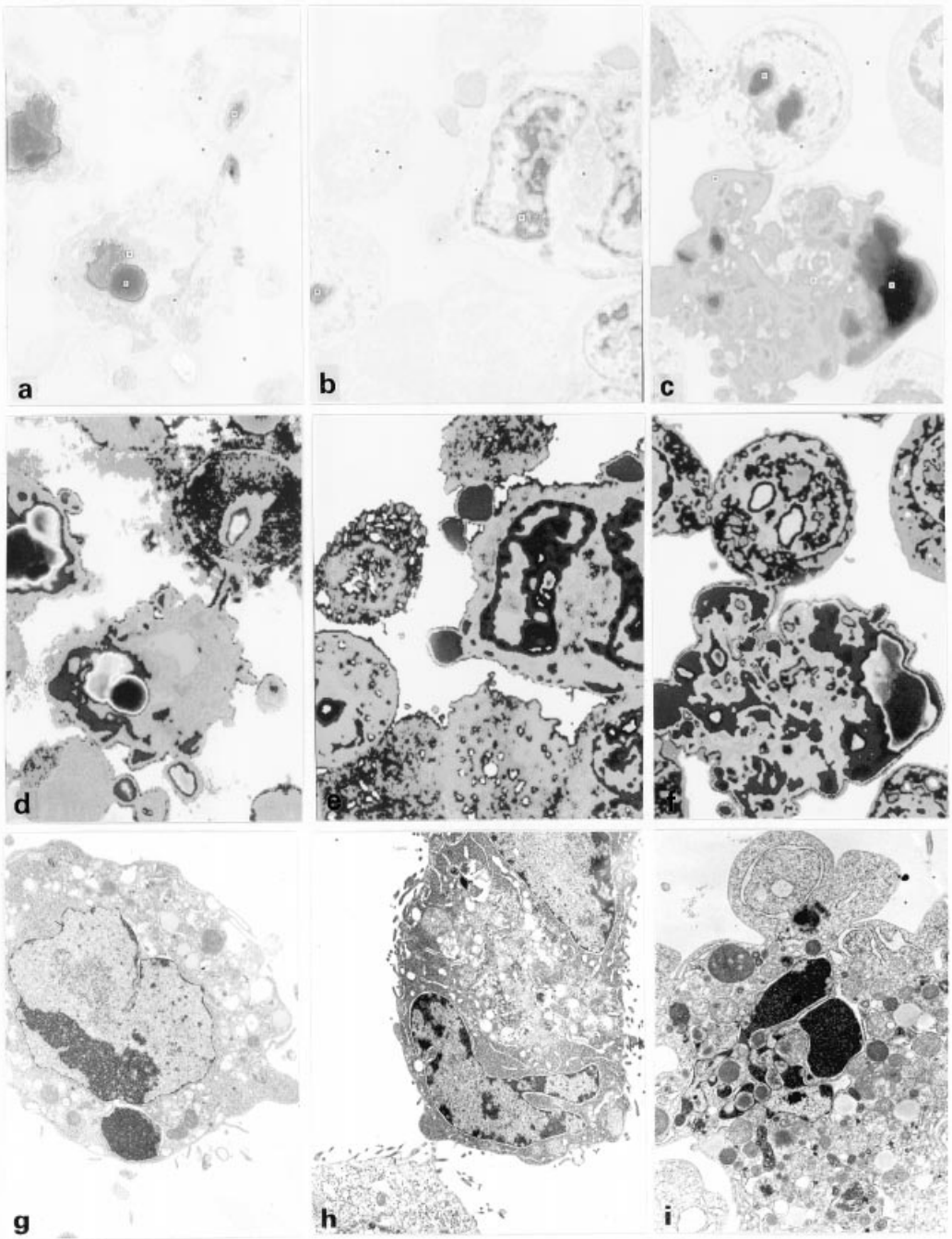
a
b
c
d
e
f
g
h
i

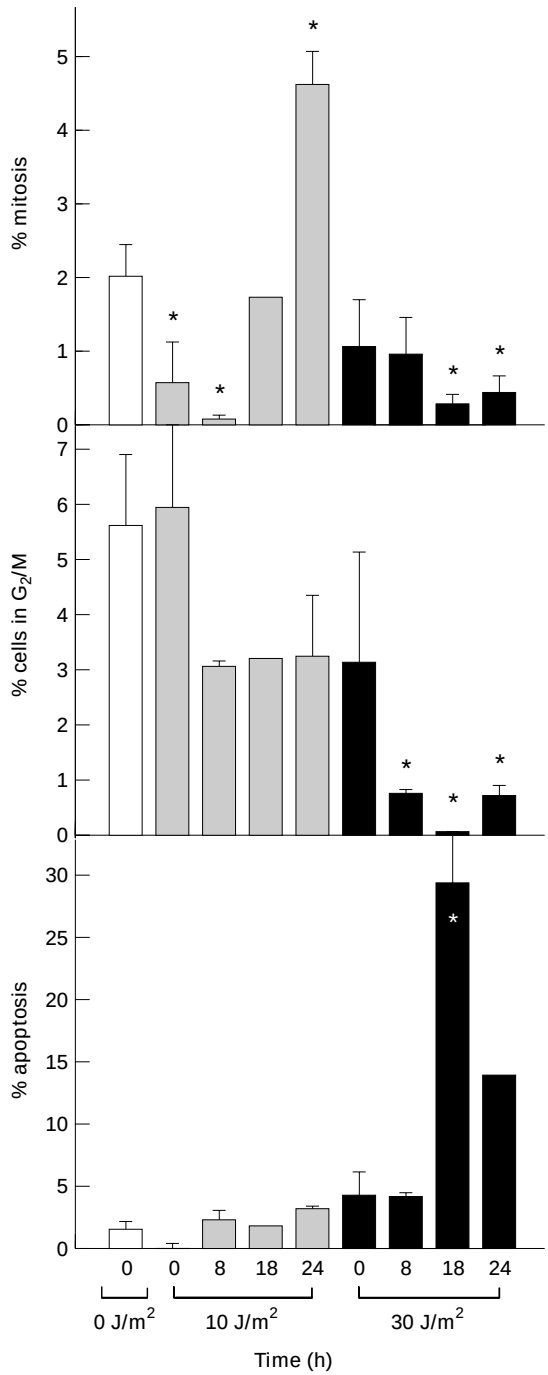

Figure 2. The percentage of cells in mitosis, G_2/M and apoptosis is shown after administration of 0, 10 and 30 J/m^2 UV-C. The cells were collected 0, 8, 18 and 24 h after treatment. Cells from the individual experiments at 0 J/m^2 UV-C group were not significantly different from each other and so were pooled as one data point.

Table 6. Percentage of HeLa cells in G_2/M†, mitosis, apoptosis and multinucleate cells from top and bottom fractions from Percoll gradients 18 h after irradiation with 30 J/m^2 UV-C

Phenotype (%)	0 J/m^2, combined	0 J/m^2, top	30 J/m^2, top	30 J/m^2, bottom
Mitotic	2.03 ± 0.5 (n=8)	2.0 (n=1)	0.39 ± 0.12 (n=5)	0* (n=4)
G_2/M	5.43 ± 1.44	1.14	0.13 ± 0.08**	0*
Apoptotic	1.94 ± 0.70	0.61	3.30 ± 1.30‡	71.48 ± 4.04***
Necrotic	0.28 ± 0.11	0	0.45 ± 0.23	0.83 ± 0.39
Dark	1.58 + 0.66	0.17	1.12 ± 0.65	0.06 ± 0.06
Multinucleate	5.0 ± 0.76	4.67	7.93 ± 4.09	4.97 ± 2.43
Amitotic	0.95 ± 0.30	1.14	0.51 ± 0.24	1.00 ± 0.11
Damage§	3.48 ± 1.28	0.78	4.88 ± 1.51	72.3 ± 4.21***

*Significantly different to column 1, 0 J/m^2 UV-C with no inhibitors, $P = < 0.05$.
**Significantly different to columns 1 and 2.
***Significantly different to columns 1, 2 and 3.
†These cells have a band of condensed chromatin which spans more than half the nuclear diameter. n=number of tissue blocks examined. Each block was sectioned several times.
‡The percentage of apoptotic HeLa cells in the top fraction after exposure to 30 J/m^2 UV-C was significantly less than the percentage of apoptoses in the combined fractions (11.05 ± 0.46). Percentage damage in combined fractions was 12.35 ± 0.86. The number of normal HeLa cells was significantly less in the bottom fraction than the top fraction 18 h after 30 J/m^2 UV-C 80.2 ± 3.63 vs. 19.89 ± 3.74, P=0.001).
§Percentage dark, necrotic and apoptotic cells together.

largely because of the impact of the increase in apoptotic cells. Apoptotic and mitotic indices and cells in G_2/M, were inversely related (Tables 6 and 7).

Characteristics of apoptotic cells

Overall, the morphology of cytoplasm, nucleus and nucleolar structures of both normal and apoptotic HeLa cells was consistent with numerous previous reports in the literature (Wyllie

Table 7. Percentage of cells in G_2/M‡, mitosis, apoptosis, and amitosis as well as pecent multinucleate, dark, necrotic and all cells with damage, in HeLa cells after irradiation with 0 or 30 J/m^2 UV-C, with and without caspase inhibitors

	0 J/m^2 UV-C		30 J/m^2 UV-C	
Phenotype (%)	No inhibitors	Inhibitors	No inhibitors	Inhibitors
Mitotic	2.03 ± 0.44 (n=9)	3.79 ± 0.51* (n=3)	0.31 ± 0.14** (n=11)	0.88 ± 0.17†* (n=3)
G_2/M‡	5.58 ± 1.28	3.92 ± 0.76	0.06 ± 0.044**	0.12 ± 0.04**
Apoptotic	1.50 ± 0.63	3.72 ± 2.98	29.5 ± 10.17†	20.22 ± 2.28†
Necrotic	0.25 ± 0.15	0.04 ± 0.04	0.63 ± 0.18††	0.40 ± 0.09
Dark	1.42 ± 0.60	0.83 + 0.23	0.64 ± 0.18	0.70 ± 0.11
Multinucleate	4.97 ± 0.37	7.81 ± 1.27	6.02 ± 2.01	6.07 ± 0.96
Amitotic	0.97 ± 0.26	1.41 ± 0.22	0.83 ± 0.19	1.21 ± 0.16
Damage§	3.18 ± 1.17	4.60 ± 2.98	30.7 ± 10.0**	21.33 ± 2.29†

*Significantly different to column 1, 0 J/m^2 UV-C with no inhibitors, $P = < 0.05$.
**Significantly different to columns 1 and 2.
†Marginally significant, P=0.1.
**, ††, etc., different than columns 1 and 2, respectively.
‡These cells have a band of condensed chromatin which spans more than half the nuclear diameter.
§Percentage dark, necrotic and apoptotic cells together.

et al. 1980, Falcieri *et al.* 1993, Lazebnik *et al.* 1993, Vitale *et al.* 1993). Spectral imaging was used to objectively characterize the morphology of these cells. Using this technique it is possible to identify the spectra of light unique to many morphological features of the stained cell. The results of this analysis indicate that each of the structural entities identified by light microscopy had mean values for spectral peaks which were significantly different from each other. The mean value for the peak of the spectra for areas of background was significantly different than all cellular components (Table 1). While some objects had spectral plots which displayed more than one peak, and were classified as different using spectral imaging, the maximum peak height was used as the primary value for Student's *t*-tests. The variation among the 5–10 pixels selected from different sites of the same structure was small (Table 1), and the spectral signatures were quite constant from cell to cell on the same slide, and from slide to slide (Table 1, Figure 1). Mean values for the spectral peaks for unaffected cytoplasm and nucleoplasm were not significantly different from each other (Table 1). Spectral imaging, however, identified the same cellular components of unaffected cells from different slides as spectrally similar and as different from apoptotic HeLa cells (Table 1; Figure 1). For example, spectra from selected pixels obtained from nucleoplasm or cytoplasm of unaffected cells were spectrally different than the spectra of cytoplasm of apoptotic cells. Dense fibrillar and granular components of the nucleolus, and the cytoplasmic ribosomes in apoptotic cells could be classified spectrally as unique structures.

Eight morphological indicators of cell damage and proliferation, and 10 structural characteristics of apoptosis were used to further define the overall response of HeLa cells to UV-C and to the two caspase inhibitors.

Cytoplasmic phenotypes

Less than 2% of the cells in the untreated cultures were apoptotic, and of these only about 2% had both the classic nuclear and cytoplasmic characteristics of apoptosis. This phenotype was present mainly in the untreated, or inhibitor treated groups without UV, and at 0 h after 30 J/m^2 irradiation (Tables 2–8). Blebbing of the cytoplasm at one pole of the cell was most common in HeLa cells treated with UV-C (Table 2). This characteristic was more common

Table 8. Common apoptotic phenotypes. Percentage of apoptotic cells with (1) rounded cytoplasm and highly fragmented chromatin; (2) cells with rounded cytoplasm and a prominent granular component; (3) rounded cytoplasm and large nucleolus with associated DNA; (4) deeply blebbed cytoplasm and highly fragmented chromatin; (5) deeply blebbed cytoplasm and a large nucleolus with associated DNA

Cytoplasm	Rounded*	Rounded	Rounded	Blebbed†	Blebbed
Nucleus	Highly fragmented DNA‡	Prominent granular component	DNA + nucleoli§	Highly fragmented DNA	DNA + nucleoli
0 J/m^2	6.7%	6.7	37.8	2.2	13.3
0 J/m^2 + Inh¶	0	29.7	20.3	0	12.2
30 J/m^2	15.1	9.3	45.6	2.5	4.7
30 J/m^2 + Inh	0.8	58.4	5.2	0.3	2.1

*Cytoplasm which is dense, full of ribosomes, but without deep cytoplasmic blebs.

†Cytoplasm which has deep indentations in the cell membrane.

‡DNA has sharp margins and appears to have been cut into oligonucleosomal size fragments.

§Large dense accumulation of nucleolar components and associated DNA, usually without fibrillar centres.

¶Inh=inhibitors of ICE, CPP32, or ICE and CPP32 together.

than deep cytoplasmic blebbing overall, however, it rarely was accompanied by nuclei with highly fragmented and condensed chromatin (Tables 2 and 8). The total number of apoptotic cells in cultures examined at 0 and 8 h after 10 J/m^2 was small, but other groups contained sufficient quantities of apoptotic cells for statistical evaluation.

The most common apoptotic phenotype after treatment with caspase inhibitors was morphologically different from the most common phenotype found in untreated and UV-treated HeLa cells (Figure 1, Tables 2–5 and 8). The granular component of the nucleolus and ribosomes in the apoptotic cytoplasm were considerably greater when cells were treated with both UV and caspase inhibitors than with UV alone. The peak of the spectral signature from the ribosomes in the cytoplasm of the apoptotic cells was not statistically significantly different from the peak of the spectrum from the granular component of the nucleolus. Nevertheless, these spectra could still be defined as distinct because of other qualities in the spectral plots (Table 1, Figure 1).

Nuclear phenotypes

HeLa cells normally have little or no condensed chromatin on their nuclear membranes. Only in the untreated cells, and cells at 24 h after 10 J/m^2 UV-C, and 8, 18 and 24 h after 30 J/m^2 UV-C were there many apoptotic figures with peripheral, highly condensed, crescent or cap-shaped DNA, typical of the digestion of DNA into oligonucleosomalsized fragments. And, only at 8 and 24 h after 10 and 30 J/m^2 UV-C did numbers of these cells exceed that of untreated controls (Table 5). The groups which received inhibitors of ICE and CPP32 did not show significant numbers of apoptotic cells with this pattern of chromatin digestion, and the predominant nuclear morphology showed a large granular component of the nucleolus and small areas of peripherally clumped DNA (Tables 3–5 and 8, Figure 1).

A large spherical condensation of the nucleolus and nucleolar-associated DNA occurred frequently in the apoptotic cells from groups treated with UV-C at early time points after irradiation (Table 4). These structures had spectral signatures of both apoptotic DNA and nucleoli (Figure 1). In cells treated with UV-C and inhibitors, DNA became condensed at the margin of the nuclear membrane, a near-normal distribution of nuclear pores at the nuclear membrane was maintained. Nuclear pores were conspicuously absent from areas of apoptotic DNA which had been digested into small fragments (Falcieri *et al.* 1994).

Small regularly spaced, peripheral clumps of condensed and partially digested chromatin in nuclei (as determined by the spectrum around 500 nm), which also contained a prominent nucleolar granular component, were most commonly features of apoptoses of cells treated with inhibitors (Table 5, Figure 1). The peak of the spectral signature of the clumps of peripherally condensed DNA was not significantly different than the apoptotic DNA found in other cells (Tables 3–6 and 8, Figure 1).

The abundance of nucleolar components in the nuclei of apoptotic cells appeared to be more common in an early stage of apoptosis (Table 8, Figure 1). Fibrillar centres were reduced in all apoptotic cells, both with and without UV irradiation. This was confirmed spectrally, by the absence of 'green' digital colouring of classified images. Less than 5% of the nuclei with digested DNA also contained nucleolar structures. There were virtually no apoptoses in the inhibitor groups, either with or without UV, which had deep cytoplasmic blebbing and highly condensed, crescentrically shaped, chromatin in pools, and none of the apoptotic figures from the 30 J/m^2 UV-C and ICE/CPP32 inhibitor group had blebbing of the entire cytoplasm.

Characteristics of cell proliferation and damage after treatment with UV-C and inhibitors of ICE and CPP32

The morphometric data from groups receiving inhibitors of ICE or CPP32 alone, or both inhibitors together were not statistically different from each other, and so were pooled into a single group ($n=3$). Additionally, except for mitotic index, where there was a significant increase in the number of cells in metaphase, data derived after the application of the protease inhibitors to HeLa cell cultures without exposure to UV-C were not different from untreated controls (Table 6, and data not shown). The mitotic indices at 18 h after 30 J/m^2 UV-C alone, and after UV-C with inhibitors, were not statistically significantly different from each other (Table 6). Thus, the increase in mitotic cells seen after treatment of unirradiated cells with protease inhibitors was completely abolished by exposure to UV.

The percentage of viable-looking mononuclear HeLa cells was lowest at 18 h after 30 J/m^2 UV-C alone (80.6% $\pm$ 0.91, controls and 57.2 $\pm$ 9.2, plus UV-C; $P=0.016$). The percentage of HeLa cells with normal morphology was 61.84% $\pm$ 3.87 in the group exposed to UV-C plus inhibitors (Table 6). The addition of inhibitors of ICE and CPP32 to the UV-C treated cultures only modestly affected measures of proliferation and damage other than apoptosis, but reduced the apoptotic index by one-third. Inhibitors administered separately, i.e. Z-VAD-FK alone and Z-DEVD-FK alone, reduced the apoptotic index in untreated controls slightly from 1.50% $\pm$ 0.63 to 0.77% and 0.70%, respectively. When these inhibitors of ICE and CPP32 were added together to unirradiated cultures, the apoptotic index rose to 9.9%, which, while not as high as following UV-C, or as statistically significant, was considerably greater than controls and opposite of the effect of either inhibitor alone. The apoptotic index and total damage (apoptotic plus dark plus necrotic cells) were increased by ICE and CPP32 inhibitors administered together to nonirradiated cells (Table 6). In contrast these were marginally effective in reversing the amount of total damage from UV-C.

DISCUSSION

The complex phenomenon of apoptosis is a topic of intense investigation (Kawabuchi *et al.* 1991, Corcoran *et al.* 1994, Baserga 1995, King & Cidlowski 1995, White 1996, Rowan & Fisher 1997, Trump *et al.* 1997). The molecular events which contribute to apoptosis are varied and numerous, and this discussion does not attempt to synthesize all that is known about apoptosis. Rather, it describes alterations in morphology which reflect interruptions of specific molecular events in apoptosis, as well as a method for detection of apoptotic DNA, and pre-ribosomal and ribosomal RNA in apoptotic cells. Many studies have used molecular tools to examine apoptosis, such as TEM, *in-situ* hybridization, immunohistochemistry, ribonuclease protection assays, genetically engineered cells and cell lines, antitumour agents and cell-free extracts (Lazebnik *et al.* 1993, Sheldrick & Carr 1993, Markovitz *et al.* 1994, Stein *et al.* 1995). Some investigators have examined the role of the caspases, which are critical to the execution of apoptosis (Lazebnik *et al.* 1993, 1994), by using protease inhibitors, However, few have used these results in tandem with morphometric, ultrastructural and spectral evaluation of the apoptotic phenotype in HeLa cells after irradiation with UV-C, as in the current study. The aims are (1) to increase our understanding of the mechanisms of apoptosis and (2) to examine a new method for identifying subcellular structures, in order to elucidate the relationships between the molecular and morphological features commonly ascribed to apoptosis. Our results support the concept that molecular events are mirrored in ultrastructural and spectral characteristics. Thus initiating apoptosis with UV-C irradiation,

and then interfering with the execution phase by inhibition of key effectors produces quantifiable differences in apoptotic morphology.

Wyllie *et al.* (1980) and others (Kawabuchi *et al.* 1991, Vitale *et al.* 1993) provided a scenario for the progression of apoptosis, where, in an early stage, chromatin was aggregated into a large compact dense mass abutting on the nuclear membrane, some of the nuclear contents were rounded, and the cytoplasm was rounded without blebs. These cells showed disruption of the cell membrane. Later stages included deep blebbing of the cytoplasm and some digestion of the DNA. The presence of peripheral, highly condensed and digested chromatin is a recognized feature of apoptosis, but may occur after other significant changes in the nuclei and nucleoli, or may not be present at all in some cell types (Cohen *et al.* 1993, Kroemer *et al.* 1995).

Less frequently in apoptotic cells, a prominent granular component was seen in nuclei which appeared to be producing large amounts of ribonucleoprotein. In the present study, this apoptotic phenotype was greatly exaggerated in cells which were irradiated and then treated with caspase inhibitors. The spectral peak for the granular component was distinct from the peak for fibrillar centres and the dense fibrillar components of the nucleolus, presumably reflecting differential uptake of osmium tetroxide and toluidine blue. It is possible that the edge effect of a small lucent fibrillar centre within the dense fibrillar portion of the nucleolus is partially responsible for the spectral differences, since intensity is a factor in determining the spectral values. Pixels selecting the granular component of the nucleolus were spectrally distinct from the cytoplasmic ribosomes, and thus could be digitially coloured accordingly. However, the peak spectral values for the two were not significantly different. Further analysis of the spectral signatures are required to explain this. Spectral examination of apoptotic cells from conventional 1 μm thick plastic sections provides a quick assay as to the number of cells in apoptosis, as well as to some specific detail about the mechanisms which execute that programme.

Rowan & Fisher (1997) divided apoptosis into four categories: trigger, modulator, effector and death. Important effectors of apoptosis belong to a group of cysteine proteases (caspases), and inhibition of caspases protects against apoptosis (Rowan & Fisher 1997). Examination of the activities of proteases indicates that it is possible to specifically block one caspase while not affecting others, suggesting that these are separate pathways in apoptosis which can operate concurrently, but independently (Lazebnik *et al.* 1995). The caspase CPP32 can cleave the enzyme poly-ADP-ribose polymerase (PARP). Cleavage of PARP is an early event in apoptosis, and inhibition of CPP32 inhibits both the cleavage of PARP as well as the induction of apoptosis (Lazebnik *et al.* 1995). In our experiments, inhibition of both CPP32 and ICE resulted in significant protection of the nucleolar structures from digestion. Spectral imaging connected the nuclear and cytoplasmic events relating to continued synthesis of ribosomes during this modified apoptosis. Failure to halt the production of pre-ribosomes would result in an increase in nucleolar size, especially in the granular component of the nucleolus, and an increase in cytoplasmic ribosomes. While experiments utilizing protease inhibitors *in vivo* must be interpreted with caution, the results of our study suggest that inhibition of caspases may not completely block apoptosis, but rather alters the timing and duration of molecular events which affect cellular phenotype, thus revealing certain morphological features which would not otherwise be observed microscopically.

In ribosomal biogenesis, the rRNA genes, rDNA transcription and the processing of the various types of ribosomal proteins and rRNA, occurs in the peripheral sites of the fibrillar centres of the nucleolus and in the dense fibrillar component (Schwartzacher & Wachtler 1993). It has been proposed that the 'very fine fibrills' (3–5 nm) represent DNA at the

margin between the fibrillar centres and the adjacent dense fibrillar component. In addition, the fibrillar centres may contain structural proteins. The dense fibrillar component is also a site of active transcription and mRNA splicing. One of the targets of caspases is the 70 kDa component of the U1 ribonucleoprotein which is involved in mRNA splicing and transport to the cytoplasm (Casciola-Rosen *et al.* 1994). It is possible that inhibition of this cleavage would allow the processing of mRNA in apoptotic cells to continue, thereby contributing to the altered morphology observed in cells treated with ICE and CPP32 inhibitors.

ICE-like proteases also cleave the nuclear structural proteins, i.e. the lamins (Lazebnik *et al.* 1995). This event, also part of the apoptotic pathway, occurs slightly later than the cleavage of PARP. The inhibition of proteases whose substrates are lamins would also contribute to the persistence of chromatin structure, and possibly slow the digestion of DNA into oligonucleosomal fragments. The inhibitors used in the current study, and others (Lazebnik *et al.* 1994, 1995) are likely to overlap with the activities and substrates of other cysteine proteases.

In conclusion, the morphometric approaches described here are sensitive to perturbations in the execution of the apoptotic pathway. Irradiation of HeLa cells with UV-C, especially when coupled with the administration of inhibitors of ICE and/or CPP32, alters the morphological characteristics of the apoptotic cell at 18 h after treatment. The results can be interpreted as showing that (1) irradiation of HeLa cells with UV-C increases the number of cells entering apoptosis; and (2) the addition of caspase inhibitors to UV-C irradiated cells interferes with the execution phase of the apoptotic process. This can be observed morphologically as a reduction in the number of cells with deep cytoplasmic blebbing, and atypical condensation of the DNA. In addition, spectral imaging, and electron microscopy, reveal an increased number of cells with abundant cytoplasmic ribosomes and large granular component of the nucleolus, suggesting that caspases are critical for terminating the biogenesis and transport of pre-rRNA and rRNA during apoptosis. The combination of biochemical and imaging approaches described here could be useful in further defining the relationship between molecular processes and cellular morphology during apoptosis.

ACKNOWLEDGEMENTS

This work was funded in part by the Center for Environmental Genetics, NIEHS ES 06096 (Dr Marshall Anderson), NIEHS ES 06636 (KD) and the Ruth Lyons Fund (MM).

REFERENCES

Afshari CA, Barrett JC. (1993) Cell cycle controls: potential targets for chemical carcinogens? *Environ. Health Perspec.* **101**(Suppl. 5), 9.

Alnemri ES, Livingston DJ, Nicholson DW *et al.* (1996) Human ICE/CE-3 protease nomenclature (letter). *Cell* **87**, 171.

Baserga R. (1995) Measuring parameters of growth. In: Rickwood D, Hames BD, eds. *Cell Growth and Paoptosis: A Practical Approach. The Practical Approach Series.* Oxford: IRL Press, Oxford University Press, 1–20.

Bishop SA, Gruffydd-Jones TJ, Harbour DA, Stokes CR. (1993) Programmed cell death (apoptosis) as a mechanism of cell death in peripheral blood mononuclear cells from cats infected with feline immunodeficiency virus (FIV). *Clin. Exp. Immunol.* **93**, 65.

Buttyan R. (1991) Genetic response of prostate cells to androgen deprivation: insights into the cellular mechanism of apoptotis. In: Tomei LD, Cope FO, eds. *Apoptosis: Basis of Cell Death, Current Communications in Cell and Molecular Biology 3.* Cold Spring Harbor, NY: Cold Spring Harbor Laboratory Press, 158.

Casciola-Rosen LA, Miller DK, Anhalt GJ, Rosen A. (1994) Specific cleavage of the 70-kDa

protein component of the U1 small nuclear ribonucleoprotein is a characteristic biochemical feature of apoptotic cell death. *J. Biol. Chem*. **269**, 30 757.

CLARK AR, PURDIE CA, HARRISON DJ *et al.* (1993) Thymocyte apoptosis induced by p53 dependent and independent pathways. *Nature* **362**, 849.

CLARKE PGH. (1990) Developmental cell death: morphological diversity and multiple mechanisms. *Anat. Embryol.* **181**, 195.

COHEN GM, SUN X-M, SNOWDEN RT, OMEROD MG, DINSDALE D. (1993) Identification of a transitional preapoptotic population of thymocytes. *J. Immunol.* **151**, 566.

COPE FO, WILLE JJ. (1991) Carcinogenesis and apoptosis: paradigms and paradoxes in cell cycle and differentiation. In: Tomei LD, Cope FO, eds. *Apoptosis: Basis of Cell Death, Current Communications in Cell and Molecular Biology 3.* Cold Spring Harbor, NY: Cold Spring Harbor Laboratory Press, 61.

CORCORAN GB, FIX L, JONES DP *et al.* (1994) Contemporary issues in toxicology. Apoptosis: molecular control point in toxicity. *Toxicol. Appl. Pharm*. **128**, 169.

DARZYNKIEWICZ Z, LI X, GONG J, HARA S, TRAGANOS F. (1995) Analysis of cell death by flow cytometry. In: Rickwood D, Hames BD, eds. *Cell Growth and Apoptosis: A Practical Approach. The Practical Approach Series.* IRL Press, Oxford: Oxford University Press, 143.

DIXON SC, SORIANO BJ, LUSH RM, BORNER MM, FIGG WD. (1997) Apoptosis: its role in the development of malignancies and its potential as a novel therapeutic target. *Ann. Pharmacother.* **31**, 76.

FALCIERI E, MARTELLI AM, BAREGGI R, CATALDI A, COCCO L. (1993) The protein kinase inhibitor ataurosporine induces morphological changes typical of apoptosis in molt-4 cells without concomitant DNA fragmentation. *Biochem. Biophys. Res. Comm*. **193**, 19.

FALCIERI E, GOBBI P, CATALDI A, ZAMAI L, FAENZA I, VITALE M. (1994) Nuclear pores in the apoptotic cell. *Histochem. J.* **26**, 754.

FORBES IJ, ZALEWSKI PD, GIANNAKIS C, COWLED PA. (1992) Induction of apoptosis in chronic lymphocytic leukemia cells and its prevention and phorbol ester. *Exp. Cell Res.* **198**, 367.

KAWABUCHI M, NAKAMURA K, HIRATA *et al.* (1991) Harmon BV Definition and incidence of apoptosis: an historical perspective. In: Tomei LD, Cope FO, eds. *Apoptosis: Basis of Cell Death, Current Communications in Cell and Molecular Biology 3.* Cold Spring Harbor, NY: Cold Spring Harbor Laboratory Press, 5.

KING KL, CIDLOWSKI JA. (1995) Cell cycle and apoptosis: common pathways to life and death. *J. Cell. Biochem*. **58**, 175.

KROEMER G, PETIT P, ZAMZAMI N, VAYSSIERE J-L, MIGNOTTE B. (1995) Biochemistry of programmed cell death. *FASEB* **9**, 1277.

LAZEBNIK Y, COLE S, COOKE CA, NELSON WG, EARNSHAW WC. (1993) Nuclear events of apoptosis in vitro in cell-free mitotic extracts: a model system for analysis of active phase of apoptosis. *J. Cell Biol.* **123**, 7.

LAZEBNIK Y, KAUFMANN SH, DESNOYERS S, POIRIER GG, EARNSHAW WC. (1994) Cleavage of poly (ADPribose) polymerase by a proteinase with properties like ICE. *Nature* (London) **371**, 346.

LAZEBNIK YA, TAKAHASHI A, MOIR RD *et al.* (1995) Studies of the lamin proteinase reveal multiple parallel biochemical pathways during apoptotic execution. *Proc. Natl. Acad. Sci.* **92**, 9042.

MARKOVITZ J, LARSEN AK, SEGAL-BENDIRDJIAN E *et al.* (1994) Inhibition of DNA topoisomerases I and II and induction of apoptosis by erbstatin and tyrphostin derivatives. *Biochem. Pharmacol.* **48**, 549.

MCDONNELL TJ. (1993) Cell division versus cell death: a functional model of multistep neoplasia. *Mol. Carcinogen.* **8**, 209.

MILLER ML, ANDRINGA A, CODY T, DIXON K, ALBERT RE. (1996) Cell proliferation and nuclear abnormalities are increased and apoptosis is decreased in the epidermis of the p53 null mouse after topical application of benzo(a)pyrene. *Cell Prolif.* **29**, 561.

NAKAYAMA K, NAKAYAMA K, NEGISH I *et al.* (1993) Disappearance of the lymphoid system in *bcl-2* homozygous mutant chimeric mice. *Science* **261**, 1584.

OMEROD MG, O'NEILL CF, ROBERTSON D, HARRAP KR. (1994) Cisplatin induces apoptosis in a human ovarian carcinoma cell line without concomitant internucleosomal degradation of DNA. *Exp. Cell Res.* **211**, 231.

RAFF MC, BARRES BA, BURNE JF, COLES HS, ISHIZAKI Y, JACOBSON MD. (1993) Programmed cell death and the control of cell survival: lessons from the nervous system. *Science* **262**, 695.

RAMACHANDRA S, STUDZINSKI GP. (1995) Morphological and biochemical criteria of apoptosis. In:

Rickwood D, Hames BD, eds. *Cell Growth and Apoptosis: A Practical Approach. The Practical Approach Series.* Oxford: IRL Press, Oxford University Press, 119.

ROWAN S, FISHER DE. (1997) Mechanisms of apoptotic cell death (review). *Leukemia* **11**, 457.

RUDIN CM, THOMPSON CB. (1997) Apoptosis and disease: regulation and clinical relevance of programmed cell death (review). *Am. Rev. Med.* **48**, 267.

SACHS L, LOTEM J. (1993) Control of programmed cell death in normal and leukemic cells: new implications of therapy. *Blood* **82**, 15.

SCHWARZACHER G, WACHTLER F. (1993) The nucleolus. *Anat. Embryol.* **188**, 515.

SHELDRICK KS, CARR AM. (1993) Feedback controls and G2 checkpoints: Fission yeasts as a model system. *BioEssays* **15**, 775.

SKEHAN P. (1995) Assays of cell growth and cytotoxicity. In: Rickwood D, Hames BD, eds. *Cell Growth and Apoptosis: A Practical Approach. The Practical Approach Series.* Oxford: IRL Press, Oxford University Press, 170.

SOLARY E, BERTRAND R, POMMIER Y. (1994) Apoptosis of human leukemic HL-60 cells induced to differentiate by phorbol ester treatment. *Leukemia* **8**, 792.

STEIN GS, STEIN JL, LIAN JB, LAST TJ, OWEN T, MCCABE L. (1995) Cell synchronization as a basis for investigating control of proliferation in mammalian cells. In: Rickwood D, Hames BD, eds. *Cell Growth and Apoptosis: A Practical Approach. The Practical Approach Series.* Oxford: IRL Press, Oxford University Press, 193.

STELLER H. (1995) Mechanisms and genes of cellular suicide. *Science* **267**, 1445.

TAYLOR R. (1993) Cell death makes for lively research. *J. NIH Res.* **5**, 59.

TEWARI M, QUAN LT, O'ROURKE K *et al.* (1995) Yama/CPP32b, a mammalian homolog of CED-3, is a CrmA-inhibitable protease that cleaves the death substrate poly(ADP-ribose) polymerase. *Cell* **81**, 801.

THOMPSON CB. (1995) Apoptosis in the pathogenesis and treatment of disease. *Science* **267**, 1456.

TOMEI LD. (1991) Apoptosis: a program for death or survival? In: Tomei LD, Cope FO, eds. *Apoptosis: Basis of Cell Death, Current Communications in Cell and Molecular Biology 3.* Cold Spring Harbor, NY: Cold Spring Harbor Laboratory Press, 279.

TOUCHETTE N. (1995) Evolutions: Apoptosis. *J. NIH Res.* **7**, 91.

TRUMP BF, BEREZESKY IK, CHANG SH, PHELPS PC. (1997) The pathways of cell death: oncosis, apoptosis, and necrosis. *Toxicologic Pathol.* **25**, 82.

VAUX DL, STRASSER A. (1996) The molecular biology of apoptosis. *Proc. Natl. Acad. Sci. USA* **93**, 2239.

VITALE M, ZAMAI L, MAZZOTTI G, CATALDI A, FALCIERI E. (1993) Differential kinetics of propidium iodide uptake in apoptotic and necrotic thymocytes. *Histochemistry* **100**, 223.

WEISS L. (1984) The Cell. In: Weiss L, ed. *Histology. Cell and Tissue Biology,* 5th edn. New York: Elsevier Biomedical, 1.

WHITE E. (1996) Overview of apoptosis. In: Apoptosis, a complete catalogue and scientific reference guide. *Calbiochemistry,* 8.

WYLLIE AH, KERR JFR, CURRIER AR. (1980) Cell death: the significance of apoptosis. *Internat. Rev. Cytol.* **68**, 251.